Fizika Nizkikh Temperatur, 2002, v. 28, No. 7, p. 745–751

Electronic structure and magneto-optical Kerr effect in the compound $UCuP_2$

O. Horpynyuk and V. V. Nemoshkalenko

Institute of Metal Physics, 36 Vernadsky Str., 252142 Kiev, Ukraine

V. N. Antonov* and B. N. Harmon

Ames Laboratory, Iowa State University, Iowa, 50011
E-mail: anton@caskad.imp.kiev.ua

A. N. Yaresko

Max Planck Institute CPFS, 40, Nöthnitzer Str., D-01187 Dresden, Germany

Received November 12, 2001

The optical and magneto-optical (MO) spectra of the ternary compound $UCuP_2$ are investigated from first principles, using the fully relativistic Dirac linear-muffin-tin-orbital band structure method and density-functional theory in the local spin-density approximation. Within a band-like description of the 5*f* electrons, good agreement with the measured MO spectra is obtained. The origin of the Kerr rotation in the compound is examined.

PACS: **71.28.+d**, 75.30.Mb

1. Introduction

Actinide compounds occupy an intermediate position between itinerant 3*d* and localized 4*f* systems [1,2], and one of the fundamental questions concerning the actinide materials is whether their *f* states are localized or itinerant. This question is most frequently answered by comparison between experimental spectroscopies and the different theoretical descriptions. Optical and magneto-optical (MO) spectroscopy, like photoelectron spectroscopy and bremsstrahlung isochromat spectroscopy, supply direct information about the energy states (both occupied and unoccupied) around the Fermi energy [3] and can provide a means of discrimination between the two theoretical limits.

Intensive experimental and theoretical study over more than two decades [4–8] has revealed that 5*f* magnetism is quite complex because Coulomb, spin–orbit, crystalline field, and exchange energies in 5*f* systems are of the same order of magnitude. Today it is well established that many unusual physical properties of the light actinide metals are a reflection of the particular nature of the 5*f* electrons. Friedel [9] proposed many years ago that the bonding in these materials must involve the 5*f* electrons. The argument for 5*f* bonding can be understood as a consequence of the extended nature of the 5*f* wave function relative to the rare-earth 4*f* wave functions. This causes them to form in bandlike states [10].

The itinerant nature of the 5*f* electrons in the light actinide metals is well known [4]. Their electronic structure and optical properties is well described by local spin-density approximation (LSDA) band structure calculations [11,12]. On the other hand, the decreasing *f*-band width (W) and the increasing intra-atomic Coulomb energy (U) results in a Mott localization between plutonium and americium [5,13,14], and the correlation effects are not properly described in the LSDA [7,15].

* Permanent address: Institute of Metal Physics, 36 Vernadsky Str., 252142 Kiev, Ukraine

Actinide compounds are excellent subjects for MO research. The participation of the 5*f* states in bonding is reflected in strongly hybridized bands near the Fermi level, with a high density of states and significant $d \rightarrow f$ oscillator strengths for optical transitions. The 5*f* delocalization favors higher magnetic ordering temperatures. In fact, many uranium compounds have ordering temperatures which are one order of magnitude higher than those in similar lanthanide compounds [3,16]. Regarding the magnitude of the MO effects compared to rare-earth materials, an enhancement due to the larger spin–orbit energy can be expected and is in part experimentally verified [3,16]. For actinide compounds the figure of merit $\sqrt{R(\theta_K^2 + \epsilon_K^2)}$, where R is the optical reflectivity and θ_K and ϵ_K are the Kerr angle and Kerr ellipticity, respectively, is one order of magnitude larger than for the best transition or rare-earth compounds [3]. Besides the issue of radioactivity (minimal for depleted uranium) a hindrance for successful application of actinide compounds in storage devices is that the typical Curie temperatures are below room temperature. This is not a fundamental problem, and can probably be overcome by suitable alloying.

For actinide materials much of the MO experimental effort up to now [3,16] has been focused on binary UX NaCl-type uranium chalcogenides (X = = S, Se, Te) and pnictides (X = P, As, Sb), uranium compounds U_3X_4 (X = P, As) with the Th_3P_4 crystal structure, and some ternary compounds such as UAsTe, the tetragonal compounds $UCuP_2$ and $UCuAs_2$, and the hexagonal compounds UCu_2P_2, UMn_2Si_2, and UMn_2Ge_2.

There are quite a few first-principle calculations of the MO spectra of uranium compounds [17–22]. The MO spectra of such compounds as UAsSe [19] and U_3P_4 [20,22] are well described in the LSDA, and we can conclude that they have at least partially itinerant electron behavior. On the other hand the MO spectra in US, USe, and UTe can be well described only in the LSDA+U approximation [21] supporting the localized description for their 5*f* electrons.

In the present work we report a detailed theoretical investigation of the electronic structure and the optical and MO Kerr properties of the ternary compound $UCuP_2$. The paper is organized as follows. The computational details are explained in Sec. 2. Section 3 presents the theoretical electronic structure and MO spectra of $UCuP_2$. The results are then compared to the experimental data. Finally, the results are summarized in Sec. 4.

2. Theoretical framework

Using straightforward symmetry considerations it can be shown that all MO phenomena are caused by the symmetry reduction — compared to the paramagnetic state — caused by magnetic ordering [23]. Concerning the optical properties this symmetry reduction only has consequences when spin-orbital (SO) coupling is considered in addition. To calculate the MO properties one therefore has to take into account the magnetism and SO coupling while at the same time dealing with the electronic structure of the material considered. In performing the corresponding band structure calculations it is normally sufficient to treat the SO coupling in a perturbative way. A more rigorous scheme, however, is obtained by starting from the Dirac equation set up in the framework of relativistic spin density functional theory [24]:

$$[c\alpha p + \beta mc^2 + IV + V_{sp}\beta\sigma_z]\psi_{n\mathbf{k}} = \epsilon_{n\mathbf{k}}\psi_{n\mathbf{k}}, \quad (1)$$

with $V_{sp}(\mathbf{r})$ the spin-polarized part of the exchange-correlation potential corresponding to the z quantization axis. All other parts of the potential are contained in $V(\mathbf{r})$. The 4×4 matrices $\boldsymbol{\alpha}$, $\boldsymbol{\beta}$, and $\mathbf{I}$ are defined by

$$\boldsymbol{\alpha} = \begin{pmatrix} 0 & \boldsymbol{\sigma} \\ \boldsymbol{\sigma} & 0 \end{pmatrix}, \ \boldsymbol{\beta} = \begin{pmatrix} \mathbf{1} & 0 \\ 0 & -\mathbf{1} \end{pmatrix}, \ \mathbf{I} = \begin{pmatrix} \mathbf{1} & 0 \\ 0 & \mathbf{1} \end{pmatrix}, \quad (2)$$

Where $\boldsymbol{\sigma}$ represents the standard Dirac matrices, and $\mathbf{1}$ is the 2×2 unit matrix.

There are quite a few band structure methods available now that are based on the above Dirac equation [25]. In the first scheme the basis functions are derived from the proper solution to the Dirac equation for the various single-site potentials [26,27]. In the second one, the basis functions are obtained initially by solving the Dirac equation without the spin-dependent term [28–30] and then this term is taken into account only in the variational step [26,31,32]. In spite of this approximation used, the second scheme nevertheless gives results in very good agreement with the first one [25], while being very simple to implement.

Phenomenologically, optical and magneto-optical properties of solids are treated by means of a dielectric tensor. The dielectric tensor is composed of the diagonal component ε_{xx} and ε_{zz} and the off-diagonal component ε_{xy} in the form

$$\varepsilon = \begin{pmatrix} \varepsilon_{xx} & \varepsilon_{xy} & 0 \\ -\varepsilon_{xy} & \varepsilon_{xx} & 0 \\ 0 & 0 & \varepsilon_{zz} \end{pmatrix}. \quad (3)$$

In the polar geometry, where the z axis is chosen to be perpendicular to the solid surface and parallel to the magnetization direction, the expression for the Kerr angle can be obtained easily for small angles and is given by [3]

$$\theta_K(\omega) + i\epsilon_K(\omega) = \frac{-\sigma_{xy}(\omega)}{\sigma_{xx}(\omega)\sqrt{1+\frac{4\pi i}{\omega}\sigma_{xx}(\omega)}}, \quad (4)$$

where θ_K is the Kerr rotation and ϵ_K is the so-called Kerr ellipticity. $\sigma_{\alpha\beta}(\alpha,\beta \equiv x,y,z)$ is the optical conductivity tensor, which is related to the dielectric tensor $\varepsilon_{\alpha\beta}$ through

$$\varepsilon_{\alpha\beta}(\omega) = \delta_{\alpha\beta} + \frac{4\pi i}{\omega}\sigma_{\alpha\beta}(\omega). \quad (5)$$

The optical conductivity tensor, or equivalently, the dielectric tensor is the important spectral quantity needed for the evaluation of the Kerr effect [33]. The optical conductivity can be computed from the energy band structure by means of the Kubo–Greenwood [34] linear-response expression [35]:

$$\sigma_{\alpha\beta}(\omega) = -\frac{ie^2}{m^2\hbar V_{uc}} \times$$

$$\times \sum_{\mathbf{k}}\sum_{nn'} \frac{f(\epsilon_{n\mathbf{k}}) - f(\epsilon_{n'\mathbf{k}})}{\omega_{nn'}(\mathbf{k})} \frac{\Pi^{\alpha}_{n'n}(\mathbf{k})\Pi^{\beta}_{nn'}(\mathbf{k})}{\omega - \omega_{nn'}(\mathbf{k}) + i\gamma}, \quad (6)$$

where $f(\epsilon_{nk})$ is the Fermi function, $\hbar\omega_{nn'}(\mathbf{k}) \equiv \epsilon_{n\mathbf{k}} - \epsilon_{n'\mathbf{k}}$ is the energy difference of the Kohn–Sham energies $\epsilon_{n\mathbf{k}}$, and γ is the lifetime parameter, which is included to describe the finite lifetime of excited Bloch electron states. The $\Pi^{\alpha}_{nn'}$ are the dipole optical transition matrix elements, which in a fully relativistic description are given by [36]

$$\mathrm{P}_{nn'}(\mathbf{k}) = m\alpha\langle\psi_{n\mathbf{k}}|c\alpha|\psi_{n'\mathbf{k}}\rangle, \quad (7)$$

where $\psi_{n\mathbf{k}}$ is the four-component Bloch electron wave function.

Equation (6) for the conductivity contains a double sum over all energy bands, which naturally separates into the so-called interband contribution, i.e., $n \neq n'$, and the intraband contribution, $n = n'$. The intraband contribution to the diagonal components of $\boldsymbol{\sigma}$ may be rewritten for zero temperature as

$$\sigma_{\alpha\alpha}(\omega) \equiv \frac{(\omega_{p,\alpha})^2}{4\pi}\frac{i}{\omega + i\gamma_D}, \quad (8)$$

where $\omega_{p,\alpha}$ are the components of the plasma frequency, which are given by

$$(\omega_{p,\alpha})^2 \equiv \frac{4\pi e^2}{m^2 V_{uc}} \sum_{n\mathbf{k}} \delta(\epsilon_{n\mathbf{k}} - E_F)\left|\Pi^{\alpha}_{nn}\right|^2, \quad (9)$$

and E_F is the Fermi energy. For cubic symmetry, we furthermore have $\omega_p^2 \equiv \omega_{p,x}^2 = \omega_{p,y}^2 = \omega_{p,z}^2$. Equation (8) is identical to the classical Drude result for the ac conductivity, with $\gamma_D = 1/\tau_D$, where τ_D is the phenomenological Drude electron relaxation time. The intraband relaxation time parameter γ_D may be different from the interband relaxation time parameter γ. The latter can be frequency dependent [37], and, because excited states always have a finite lifetime, will be nonzero, whereas γ_D will approach zero for very pure materials. Here we adopt the perfect crystal approximation, i.e., $\gamma_D \to 0$. For the interband relaxation parameter, on the other hand, we shall use, unless stated otherwise, $\gamma = 0.4$ eV. This value has been found to be on average a good estimate of this phenomenological parameter. The contribution of intraband transitions to the off-diagonal conductivity usually is not considered. Also, we did not study the influence of local field effects on the MO properties.

We mention, lastly, that the Kramers–Kronig transformation has been used to calculate the dispersive parts of the optical conductivity from the absorptive parts.

3. Crystal structure and computational details

Self-consistent energy band-structure calculations of $UCuP_2$ were performed by means of the fully relativistic, spin-polarized linear-muffin-tin-orbital (SPR LMTO) method using the atomic sphere approximation with combined corrections included [26,29–32]. The LSDA part of the energy band structure calculations were based on the spin-density-functinal theory with von Barth–Hedin parameterization [38] of the exchange-correlation potential. Core charge densities were recalculated at every iteration of the self-consistency loop. The **k**-space integrations were performed with the improved tetrahedron method [39] and the charge was obtained self-consistently with 349 irreducible k points. The basis consisted of U *s, p, d, f,* and *g*; Cu *s, p, d*, and *f* ; P *s, p*, and *d* LMTOs.The energy expansion parameters $E_{\nu Rl}$ were chosen at the centers of gravity of the occupied parts of the partial state densities; this gives high accuracy for the charge density.

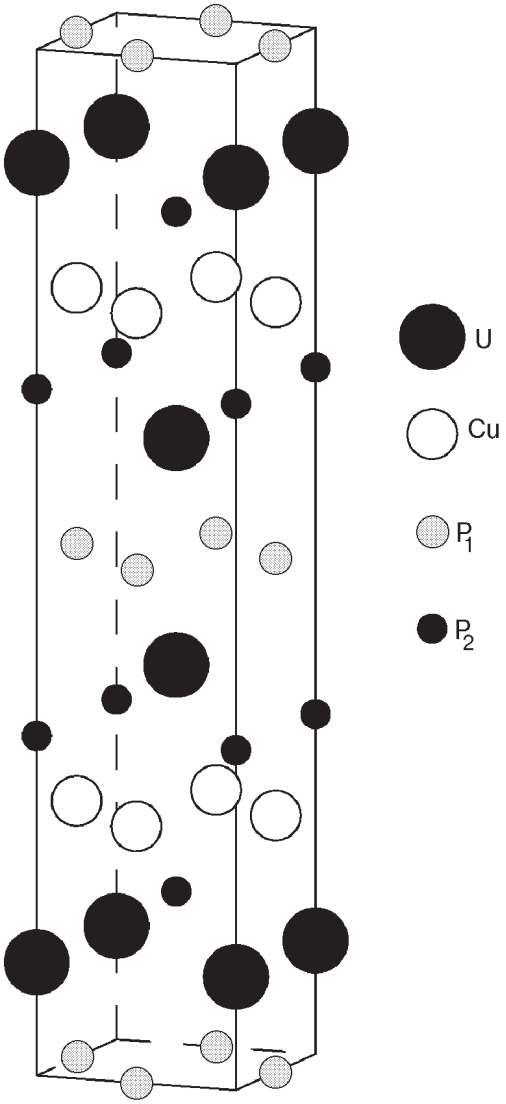

Fig. 1. Crystal structure of tetragonal $UCuP_2$.

$UCuP_2$ belongs to the layered tetragonal $ZrAl_3$ type crystal structure (Fig. 1) with the space group $I4/mmm$ (No. 139) with U at the 4*e* position, Cu at the 4*d* position, and P at the 4*c* and 4*e* positions. The phosphorus atoms have two nonequivalent positions: the plane with P_1 atoms is situated between uranium planes, while the plane containing the P_2 atoms lies between uranium and copper planes (see Fig. 1). The lattice constants are a = 3.803 Å, c = = 18.523 Å [40]. The corresponding Brillouin zone is shown in Fig. 2. The unit cell of $UCuP_2$ contains 8 atoms.

4. Results and discussion

The uranium pnictide ternary compounds with copper or nickel crystallize in a high-symmetry

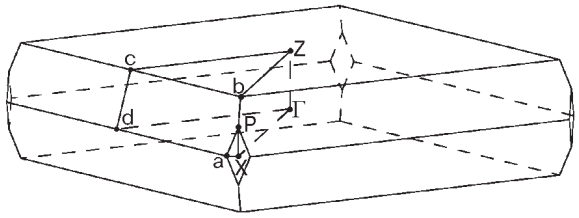

Fig. 2. Brillouin zone of tetragonal $UCuP_2$.

structure: $UCuP_2$, $UCuAs_2$, and $UNiAs_2$ are tetragonal [41] and UCu_2P_2 and UCu_2As_2 are hexagonal [42]. The U–Cu ternaries order ferromagnetically, in contrast to the U–Ni ternaries, which are all antiferromagnets [3]. The magnetic ordering temperatures are among the highest known so far for uranium compounds, reaching 216 K for UCu_2P_2 [43]. The magnetic and transport properties of $UCuP_2$ were investigated by Kaszorowski et al. [44] on single-crystal specimens. They found that the compound is ferromagnetic below 75 K, with a spontaneous magnetic moment of 0.98 μ_B, and in the magnetically ordered region it exhibits large magnetocrystalline anisotropy constants. The electrical resistivity of $UCuP_2$ at low temperature behaves as T^2, while in the temperature range above T_C the observed negative slope of $\rho(T)$ may point to Kondo lattice behavior [44].

The energy dependence of the Kerr rotation and ellipticity of $UCuP_2$ have been measured by Funagalli et al. [45]. The measurements were done on a natural grown surface perpendicular to the *c* axis. Although $UCuP_2$ has a lower uranium concentration in comparison with UX and U_3X_4 (X = P, As) compounds, its Kerr rotation reaches 1.6° (Ref. 45).

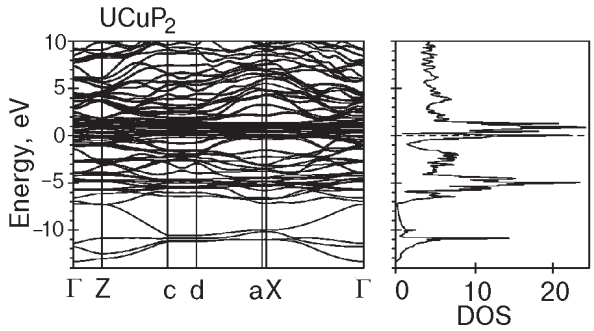

Fig. 3. Self-consistent fully relativistic, spin-polarized energy band structure and total DOS (in states/(unit cell eV)) of $UCuP_2$.

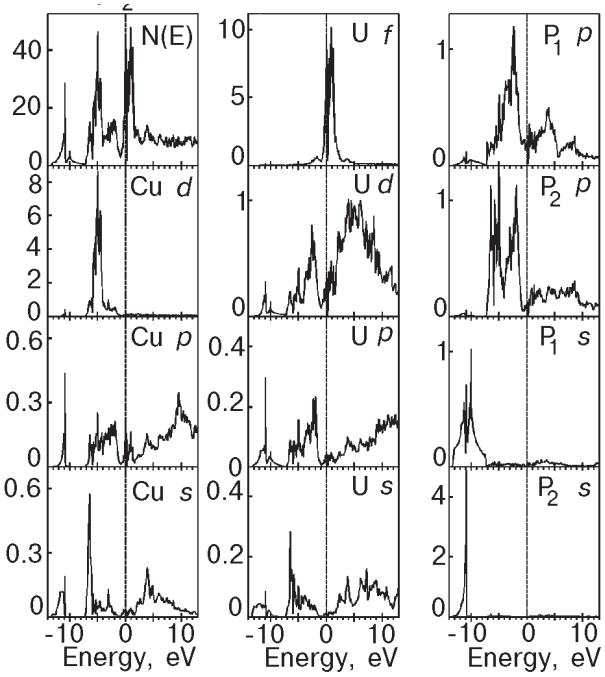

Fig. 4. Fully relativistic, spin-polarized total (in states/(unit cell eV)) and partial densities of state (in states/(atom eV)) calculated for $UCuP_2$.

The fully relativistic spin-polarized energy band structure of ferromagnetic $UCuP_2$, shown in Fig. 3, is rather complicated. It may, however, be understood from the total and partial density of states (DOS) presented in Fig. 4. The bands in the lowest region between –13.4 and –7.2 eV have mostly a P *s* character with some amount of U and Cu *spd* character mixed in. The energy bands between –7.2 and –0.4 eV are P 3*p* states strongly hybridized with the Cu 3*d* and U 6*d* states. There is a quasi-gap between P *s* and *p* states. The Cu 3*d* states are fully occupied and situated around 5.0 eV below the Fermi level. The U 5*f* energy bands are located above and below E_F at about –0.4 to 3.0 eV. The highest region above the Fermi energy can be characterized as anti-bonding U 6*d* states. It is interesting to note that the 3*p* partial density of states for P_1 and P_2 sites differ from each other significantly. This reflects the different positions for the two phosphorus atoms. As we mentioned above, the plane with P_1 atoms is situated between uranium planes, whereas the plane with P_2 atoms lies between uranium and copper planes (see Fig. 1). The P_1 atoms have as neighbors four P_1 atoms at a distance of 2.688 Å and four uranium atoms at 2.793 Å. On the other hand, the P_2 atoms have four Cu neighbor atoms at a distance of 2.423 Å and four uranium atoms at 2.898 Å. As a result, the 3*p* partial density of states for the P_1 site has one peak structure for occupied states, reflecting strong hybridization between the P_1 *3p* and U *6d* states, whereas the 3*p* partial density of states for the P_2 site has two peaks due to the hybridization of P_2 3*p* states with both Cu 3*d* and U 6*d* states.

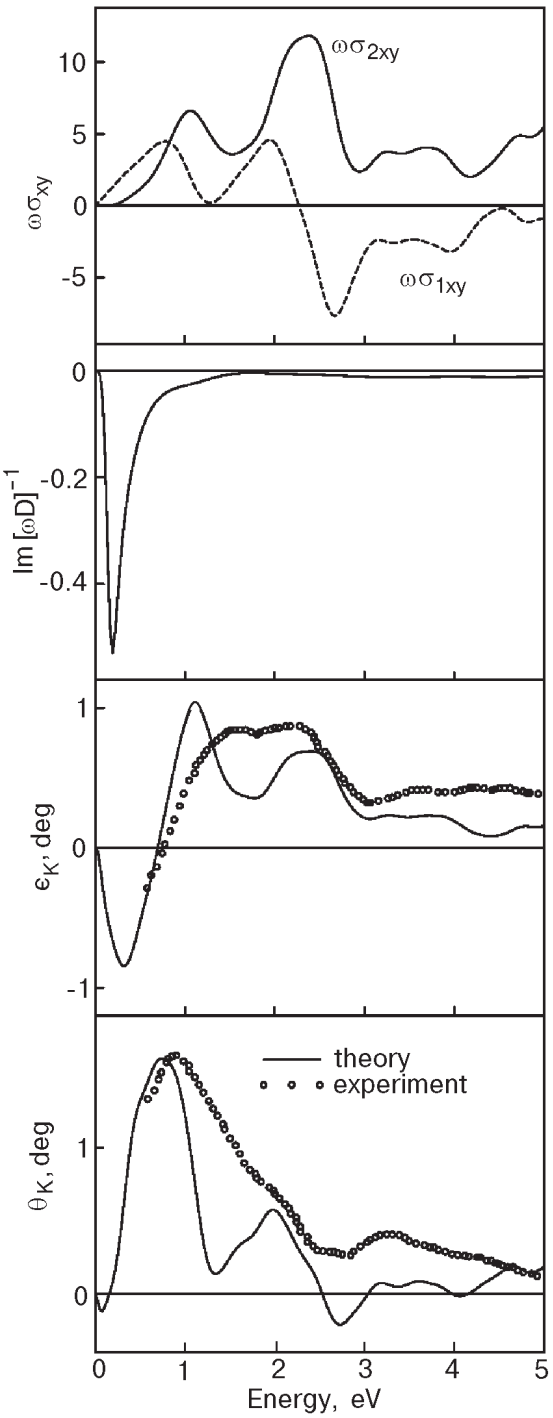

Fig. 5. Calculated and experimental [45] Kerr rotation (θ_K) and Kerr ellipticity (ϵ_K) spectra of $UCuP_2$ as well as the theoretically calculated off-diagonal optical conductivity σ_{xy} and function Im $[\omega D]^{-1}$ (see the explanation in the text).

After consideration of the above band structure properties we turn to the MO spectra. In Fig. 5 we show the calculated and experimental [45] MO Kerr spectra of $UCuP_2$. There exists rather good agreement between the experimental Kerr spectra and the *ab initio* LSDA calculated one. Overall, the experimental features are reasonably well reproduced, except the theoretically calculated spectra have sharper features in comparison with the experimentally observed spectra. There is also a small red energy shift by about 0.1 eV in the position of the main Kerr rotation and ellipticity peaks in comparison with the experiment. We can conclude, therefore, that the spectral behavior of the MO Kerr spectra in $UCuP_2$ is well described by LSDA band-structure theory.

To investigate the origin of the Kerr spectra, we consider the separate contributions of both the numerator of Eq. (4), i.e., $\sigma_{xy}(\omega)$ and the denominator, $D(\omega) \equiv \sigma_{xx}\sqrt{1+(4\pi i / \omega)\sigma_{xx}}$. In Fig. 5 we show how the separate contributions of numerator and denominator bring about the Kerr angle and Kerr ellipticity of $UCuP_2$. The imaginary part of the inverse denominator (times the photon frequency), $\mathrm{Im}[\omega D]^{-1}$, displays a strong resonance structure at about 0.2 eV. However, the imaginary and real parts of $\omega\sigma_{xy}$, i.e. $\omega\sigma_{2xy}$ and $\omega\sigma_{1xy}$, display a very small value at this energy. Therefore the first minimum in the Kerr rotation and Kerr ellipticity at around 0.2 eV results from a deep resonance structure of the denominator. Outside the infrared peak, for energies above 0.5 eV, the Kerr rotation and ellipticity spectra are fully determined by the shape of σ_{xy}, which in turn are known to be due to the interplay of SO coupling and spin polarization. The two peaks at about 0.7 and 2.0 eV in the Kerr rotation spectrum originate mostly from U $6d \to 5f$ interband transitions (see Figs. 3 and 4). The interband transitions from the Cu $3d$ to the U $5f$ band start above 4 eV. In the 1 to 5 eV energy region the theoretical and experimental curves deviate from one another in some details.

The theoretically calculated figure of merit $\sqrt{R(\theta_K^2+\epsilon_K^2)}$ in $UCuP_2$ has a maximum value of 1.2° at 0.7 eV, which is higher than that in PtMnSb (0.83° at 1.57 eV) [46] but smaller than that in U_3As_4 (6.0° at 0.35 eV) [22].

In spite of the reasonably close correspondence between the experimental and theoretical Kerr spectra, we find that not all properties of $UCuP_2$ are equally well represented. For example, the calculated total magnetic moment of uranium in $UCuP_2$ is only $0.262\mu_B$ (Table) (with spin moment $-0.886\mu_B$ and orbital moment $1.148\mu_B$), which is considerably smaller than the experimental moment of about $0.89\ \mu_B$ [44].

Table

The experimental and LSDA calculated spin, orbital and total magnetic moments (in μ_B) of $UCuP_2$.The experimental data are from Ref. 44

Atom	M_s	M_l	M_{total}	Experiment.
U	−0.886	1.148	0.262	0.89
Cu	−0.009	−0.002	−0.011	
P_1	0.012	0.001	0.013	
P_2	−0.006	−0.001	−0.007	

The calculated moment is dominated by $5f$ states: the $5f$ components of the spin and orbital moment are $-0.845\mu_B$ and $1.137\mu_B$, respectively. It is a well-known fact, however, that within the LSDA the total magnetic moment of uranium compounds in general comes out too small [47–51]. Corrections which simulate Hund's second rule interactions in solids, describing orbital correlations absent in the homogeneous electron gas, such as the orbital polarization (OP), are needed to bring the magnetic moment into better agreement with experiment [48–51]. Interestingly, the fact that the OP is too small within the LSDA does not preclude a reasonable explanation of the MO Kerr spectrum. The same conclusion was also reached previously for UAsSe [19] and U_3X_4 (X = P, As, Sb, and Bi) [22] compounds.

5. Summary

On the basis of the good agreement between experimental and theoretical MO characteristics we conclude that the U $5f$ electrons in the ternary $UCuP_2$ compound are essentially itinerant. However, the difference in the main peak position of the Kerr rotation and ellipticity spectra requires further investigation of the electron self-energies.

1. J. D. Becker, J. M. Wills, L. Cox, and B. R. Cooper, *Phys. Rev.* **B54,** 17265R (1996).
2. L. M. Sandratskii and J. Kübler, *Phys. Rev.* **B55**, 11395 (1997).
3. W. Reim and J. Schöenes, in *Ferromagnetic Materials*, E. P. Wohlfarth and K. H. J. Buschow (eds.), North-Holland, Amsterdam (1990), Vol. 5, p. 133.
4. A. J. Freeman and D. D. Koelling, *The Actinides: Electronic Structure and Related Properties*,

A. J. Freeman and J. E. Darby (eds.), Academic Press, New York (1974), Vol. 1; E. Warren, E. Picket, A. J. Freeman, and D. D. Koelling, *Phys. Rev.* **B22**, 2965 (1980).
5. B. Johansson, *Phys. Rev.* **B11**, 2740 (1975).
6. H. I. Skriver, O. K. Andersen, and B. Johansson, *Phys. Rev. Lett.* **41**, 42 (1978); *ibid.* **44**, 1230 (1980).
7. M. S. S. Brooks, *J. Magn. Magn. Mater.* **29**, 257 (1982); *J. Phys.* **F13**, 103 (1983).
8. *Handbook of Physics and Chemistry of the Actinides*, A. J. Freeman and G. H. Lander (eds.), North-Holland, Amsterdam (1984).
9. J. Friedel, *J. Phys. Chem. Solids* **1**, 175 (1956).
10. R. C. Albers, A. M. Boring, J. M. Wills, L. E. Cox, O. E. Eriksson, and N. E. Christensen, *Phys. Rev.* **B54** , 14405 (1996).
11. V. N. Antonov, A. I. Bagljuk, A. Ya. Perlov, V. V. Nemoshkalenko, Vl. N. Antonov, O. K. Andersen, and O. Jepsen, *Fiz. Nizk, Temp.* **19**, 689 (1993) [*Sov. J. Low Temp. Phys.* **19**, 792 (1993)].
12. T. Gasche, M. S. S. Brooks, and B. Johansson, *Phys. Rev.* **B54**, 2446 (1996).
13. J. Kollar, L. Vitos, and H. L. Skriver, *Phys. Rev.* **B55**, 15353 (1997).
14. P. Söderlind, J. M. Wills, B. Johansson, and O. Eriksson, *Phys. Rev.* **B55**, 1997 (1997).
15. J. van Ek, P. A. Sterne, and A. Gonis, *Phys. Rev.* **B48**, 16280 (1993).
16. W. Reim, *J. Magn. Magn. Mater.* **58**, 1 (1986).
17. T. Kraft, P. M. Oppeneer, V. N. Antonov, and H. Eschrig, *Phys. Rev.* **B52**, 3561 (1995).
18. B. R. Cooper, S. P. Lim, I. Avgin, Q. G. Sheng, and D. L. Price, *J. Phys. Chem. Solids* **56**, 1509 (1995).
19. P. M. Oppeneer, M. S. S. Brooks, V. N. Antonov, T. Kraft, and H. Eschrig, *Phys. Rev.* **B53**, 10437R (1996).
20. J. Köhler, L. M. Sandratskii, and J. Käber, *Phys. Rev.* **B55**, 10153R (1997).
21. P. M. Oppeneer, V. N. Antonov, A. Ya. Perlov, A. N. Yaresko, T. Kraft, and H. Eschrig, *Physica* **B230–232**, 544 (1997).
22. V. N. Antonov, B. N. Harmon, A. N.Yaresko, and A.Ya. Perlov, *Phys. Rev.* **B59**, 14571 (1999).
23. W. H. Kleiner, *Phys. Rev.* **142**, 318 (1966).
24. A. H. MacDonald and S. H. Vosko, *J. Phys. C: Solid State Phys.* **12**, 2977 (1979).
25. H. Ebert, H. Freyer, A. Vernes, and G.-Y. Guo, *Phys. Rev.* **B53**, 7721 (1996).
26. H. Ebert, *Phys. Rev.* **B38**, 9390 (1988).
27. I. V. Solovyev, A. B. Shik, V. P. Antropov, A. I. Liechtenstein, V. A. Gubanov, and O. K. Andersen, *Sov. Phys. Solid State* **31**, 1285 (1989)
28. D. D. Koelling and B. N. Harmon, *J. Phys. C: Solid State Phys.* **10**, 3107 (1977)
29. O. K. Andersen, *Phys. Rev.* **B12**, 3060 (1975).
30. V. V. Nemoshkalenko, A. E. Krasovskii, V. N. Antonov, Vl. N. Antonov, U. Fleck, H. Wonn, and P. Ziesche, *Phys. Status Solidi* **B120**, 283 (1983).
31. V. N. Antonov, A. Ya. Perlov, A. P. Shpak, and A. N. Yaresko, *J. Magn. Magn. Mater.* **146**, 205 (1995).
32. V. V. Nemoshkalenko and V. N. Antonov, *Computational Methods in Solid State Physics*, Gordon and Breach, London (1998).
33. J. Schoenes, in: *Materials Science and Technology*, Vol. 3A: *Electronic and Magnetic Properties of Metals and Ceramics,* Verlag Chemie, Weinheim (1992), p. 147.
34. R. Kubo, *J. Phys. Soc. Jpn.* **12**, 570 (1957)
35. C. S. Wang and J. Callaway, *Phys. Rev.* **B9**, 4897 (1974)
36. V. N. Antonov, A. I. Bagljuk, A. Ya. Perlov, V. V. Nemoshkalenko, Vl. N. Antonov, O. K. Andersen, and O. Jepsen, *Low Temp. Phys.* **19**, 494 (1993).
37. A. Santoni and F. J. Himpsel, *Phys. Rev.* **B43**, 1305 (1991).
38. U. von Barth and L. A. Hedin, *J. Phys. C: Solid State Phys.* **5**, 1692 (1972).
39. P. E. Blöchl, O. Jepsen, and O. K. Andersen, *Phys. Rev.* **B49**, 16223 (1994).
40. P. Villars and L. D. Calvert, *Pearson's Handbook of Crystallographic Data for Intermetallic Phases*, ASM International, Materials Park (1991).
41. Z. Zolnierek, D. Kaczorowski, and R. Troc, *J. Less-Common. Met.* **128**, 265 (1987).
42. Z. Zolnierek, H. Nöel, and D. Kaczorowski, *J. Less-Common. Met.* **132**, 265 (1987).
43. Z. Zolnierek, D. Kaczorowski, R. Troc, and H. Nöel, *J. Less-Common. Met.* **121**, 193 (1986).
44. D. Kaczowski, R. Troc, and H. Nöel, *J. Phys. Condens. Matter* **3**, 4959 (1991).
45. P. Fumagalli, J. Schöenes, and D. Kaczorowski, *Solid State Commun.* **65**, 173 (1988).
46. H. Ikekame, K. Sato, K. Takanashi, and H. Fujimori, *Jpn. Appl. Phys.* **32**, 284 (1993).
47. M. S. S. Brooks and B. Johansson, in: *Handook of Magetic Mateials*, K. H. J. Buschow (ed.), North-Holland, Amsterdam (1993), vol. 7, p. 139.
48. M. S. S. Brooks, *Physica* **B130**, 6 (1985).
49. O. Eriksson, M. S. S. Brooks, and B. Johansson, *Phys. Rev.* **B41**, 7311 (1990).
50. L. Severin, M. S. S. Brooks, and B. Johansson, *Phys. Rev. Lett.* **B71**, 3214 (1993).
51. A. Mavromaras, L. Sandratskii, and J. Kübler, *Solid State Commun.* **106**, 115 (1998).